Journal of Fluids and Structures 40 (2013) 317–336

Contents lists available at SciVerse ScienceDirect

Journal of Fluids and Structures

journal homepage: www.elsevier.com/locate/jfs

# Two-dimensional water entry and exit of a body whose shape varies in time

A. Tassin [a,*], D.J. Piro [b], A.A. Korobkin [a], K.J. Maki [b], M.J. Cooker [a]

[a] School of Mathematics, University of East Anglia, Norwich Research Park, Norwich NR4 7TJ, United Kingdom
[b] Department of Naval Architecture and Marine Engineering, University of Michigan, Ann Arbor, MI 48109, United States

ARTICLE INFO

*Article history:*
Received 5 December 2012
Accepted 6 May 2013
Available online 13 June 2013

*Keywords:*
Water entry
Water exit
Fluid–structure interaction
Wagner theory
Modified Logvinovich model
CFD

ABSTRACT

The two-dimensional water entry and exit of a body whose shape varies in time in a prescribed way is investigated through analytical and numerical modelling. For this purpose, an analytical model has been developed which extends the modified Logvinovich model of water impact to bodies with time-varying shape. A modified von Karman approach has been developed to describe the exit stage, and a rational derivation of the water exit model which is in use in offshore engineering is presented. CFD simulations are used to assess the accuracy of the analytical model. Several case studies of water entry and exit are presented. The analytical model provides very good force predictions during the entry stage in all cases, but the accuracy of the model in the exit stage depends on the maximum penetration depth. In particular, the appearance of high fluid forces on the body directed downward in both the entry and exit stages is remarkable.



## 1. Introduction

Studies on violent free-surface flows are motivated by various industrial applications from different areas. In coastal and offshore engineering, one may be concerned by water-wave impacts on structures (see Faltinsen et al., 2004; Peregrine, 2003). In the marine industry, water impacts such as sloshing, slamming and water on deck are of important concern as they induce critical loads on marine structures (see Faltinsen et al., 2004; Faltinsen and Timokha, 2009; Kapsenberg, 2011). Substantial work has also been done on water entry with applications to aerospace structures (see Seddon and Moatamedi, 2006 for an overview). The pioneering work of von Karman (1929) and Wagner (1932) (see also Wagner, 1931) on water impact modelling was motivated by the landing of seaplanes. These days the aeronautical industry is strongly concerned by water impacts during emergency landing on water (ditching), see Bensch et al. (2001), Climent et al. (2006) and Toso (2009). Some military applications also involve high-speed free-surface piercing bodies like the water entry and exit of missiles. Ricochet and bouncing of projectiles are also interesting violent free-surface flows, involving water entry and subsequent water exit (see Hicks and Smith, 2011; Truscott et al., 2009).

Water impacts offer many challenges to hydrodynamicists in terms of modelling. Indeed, despite the present high level of development of Computational Fluid Dynamics (CFD) techniques, the numerical simulation of water-impact related problems remains difficult because of the presence of moving boundaries, very localised high-pressure zones and small scale phenomena such as thin splash jets. In particular, it is difficult to accurately predict the pressure distributions due to

* Corresponding author. Tel.: +44 1603591373.
*E-mail addresses:* a.tassin@uea.ac.uk, alantassin@yahoo.fr (A. Tassin), djpiro@umich.edu (D.J. Piro), a.korobkin@uea.ac.uk (A.A. Korobkin), kjmaki@umich.edu (K.J. Maki), m.cooker@uea.ac.uk (M.J. Cooker).

0889-9746/$ - see front matter © 2013 Elsevier Ltd. All rights reserved.
http://dx.doi.org/10.1016/j.jfluidstructs.2013.05.002

high levels of noise induced by the numerical algorithms used to model the fluid–structure interaction. Obtaining reliable CFD results becomes even more difficult when additional physical phenomena affect the results: deformation of the structure, air-cushioning, ventilation, fluid compressibility and cavitation.

Experimental studies on water impact are therefore very important for the validation of numerical simulations and analytical models, but they also present difficulties (see Kapsenberg, 2011). In particular, pressure measurements are very sensitive to small details of impact (see Haboussa et al., 2008; Kaminski and Bogaert, 2009), and therefore, measuring the resultant hydrodynamic forces at given speeds might be more reliable (see El Malki Alaoui et al., 2012). A few full scale experiments have been carried out in the ship industry. However, the full scale ditching of an instrumented aircraft might present prohibitive cost and safety issues.

Although analytical models of water impact can be seen as less flexible than CFD, they can offer an interesting alternative to CFD and experiments. Analytical models are usually viewed as complementary to CFD and experiments, and are commonly employed to assess the accuracy of CFD techniques. For examples see Aquelet et al. (2006), Gong et al. (2009), Oger et al. (2006) and Qian et al. (2006). Moreover, the robustness and the lower computational cost of analytical approaches make them attractive for practical applications. Indeed, the analytical theory introduced by Wagner (1931), the so-called original Wagner model, is still widely used in the ship industry to estimate slamming loads. In addition, from the assumptions of Wagner (potential flow theory and linearisation of the boundary conditions), various analytical and semi-analytical models of water impact have been derived in order to enhance the accuracy and the domain of validity of the Wagner model. A better description of the pressure distribution in the vicinity of the splash jet has been obtained by the use of matched asymptotic expansions, as shown by Wagner (1932), Cointe and Armand (1987) and Howison et al. (1991). Zhao et al. (1997) introduced a generalised Wagner model in which the pressure is computed according to the nonlinear Bernoulli equation and the exact kinematic boundary condition is satisfied in the computation of the velocity potential. The generalised Wagner model shows great improvements in terms of force prediction. This is especially true for large deadrise angles, where the force is overestimated by the original Wagner model. Later, Korobkin (2004) observed that a similar improvement had been obtained by Vorus (1996) using the flat-disc approximation together with the nonlinear dynamic free-surface condition. The common feature of the Vorus model and the generalised Wagner model is the use of the nonlinear Bernoulli equation, so Korobkin (2004) proposed the Modified Logvinovich Model (MLM) in which the pressure on the body is computed using the nonlinear Bernoulli equation, and the velocity potential on the body boundary is approximated by a Taylor expansion of the velocity potential of the original Wagner model (see details in Section 2). The computational cost of the MLM is therefore lower than that of the generalised Wagner model or the Vorus model, and it gives accurate results in terms of force for relatively large deadrise angles, as reported by Korobkin (2004) and Tassin et al. (2010). The MLM has been used to study the impact of bodies with asymmetric contours by Korobkin and Malenica (2005) and the impact of a wedge with roll motion by Qin et al. (2011). Moreover, a three-dimensional version of the MLM was proposed by Korobkin (2005) and developed further by Tassin et al. (2012). Progress has also been made on three-dimensional analytical models of water impact by Scolan and Korobkin (2001), Gazzola (2007) and Tassin et al. (2012). Furthermore, examples of analytical water impact models including hydroelastic coupling, ventilation, aeration, cavitation or separation have been reported by Scolan (2004), Gazzola and de Lauzon (2008), Khabakhpasheva and Korobkin (2013), Semenov and Yoon (2009), Korobkin (2006), Takagi (2004), Khabakhpasheva et al. (2013) and Reinhard et al. (2011).

In this paper, we consider the two-dimensional analytical and numerical modelling of the partial water entry and subsequent partial exit of a body. The body goes through a water entry stage followed by a water exit stage. This study is restricted to relatively small penetration depths compared with the wetted width, so there is no air cavity behind the body and the upper part of the body remains dry. The exit phenomenon is therefore rather different from the water exit of a body which is initially totally submerged, as considered in Greenhow (1988). Also, in contrast to the study of Greenhow (1987), the deadrise angle of the body is small enough that the water entry stage can be treated as an impact. In addition, in the present analysis, the shape of the body can change in time. The body is symmetric about a vertical plane. The development of a semi-analytical model of water entry and exit is first motivated by the extension of the $2D+t$ approach (strip method) used in the naval industry for the design of planing hulls to more general body shapes such as an aircraft fuselage (for ditching applications). In contrast to the geometry of typical planing hulls which are rather prismatic (see Iafrati and Broglia, 2008), the curvature of an aircraft fuselage is much more pronounced. Therefore, instead of reducing the three-dimensional water impact problem to the water entry of a wedge at constant speed, the $2D+t$ approach reduces the three-dimensional impact of a curved hull to the water entry and exit of a body whose shape varies in time. For example, as illustrated in Fig. 1, the $2D+t$ analysis of an ellipsoid of revolution moving horizontally at a fixed penetration depth in water leads to the study of the water entry and exit of a circular cylinder whose radius is changing in time (first expanding and then contracting). The analytical approach developed in this study can be extended to hydroelastic problems involving water entry and exit, as presented in Piro and Maki (2013b). Moreover, this approach can be used to study other problems involving the water entry of bodies whose shape is changing such as the compliant-hull concept for planing craft studied by Vorus (2004) to reduce wave-impact shocks.

In contrast to the extensive research on the water entry problem, very little work has been dedicated to the water exit problem. As a consequence, the water exit problem is not as well formulated as the water entry problem via the Wagner theory and contradictory arguments can be found in the literature. The difficulties arise from the de-wetting phenomenon: as the body moves away from the liquid, the surface of the body in contact with the fluid (the wetted area) contracts. Some of the water particles are leaving the body surface and the parameters governing this phenomenon are not clearly identified.

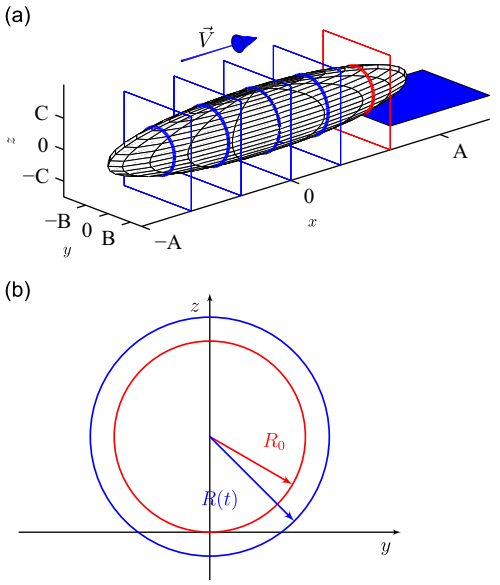


**Fig. 1.** 2*D*+*t* analysis of an ellipsoid of revolution of semi-axis *A*, *B* and *C* moving horizontally in the *x*-direction. (a) Three-dimensional view of the 2*D*+*t* decomposition (initial free surface level depicted in blue) and (b) 2-D water entry and exit problem in the first control plane in contact with the water surface. (For interpretation of the references to color in this figure caption, the reader is referred to the web version of this article.)

Indeed, enforcing a non-penetration condition on the body surface under a high pressure during the entry stage is easier to treat than deciding whether a fluid particle should leave the surface of the rising body as the pressure drops below atmospheric pressure, or remain attached to the body surface. Similarities can be found between the de-wetting phenomenon and the separation phenomenon that might occur during the water impact of a curved body. Indeed, during the water impact of a curved body, the wetted area may expand without reaching the maximum breadth of the body (see Lin and Shieh, 1997). Experiments on the water entry of spheres have shown that the wetting properties of the body surface strongly affected the separation, and the presence or absence of cavity formation (see Duez et al., 2008; Techet and Truscott, 2011). To our knowledge, the only reported experiment designed to measure the hydrodynamic force during the water exit of a floating body has been made by Tveitnes et al. (2008). However, Piro and Maki (2012) showed by a CFD investigation that in the conditions of the experiments, the flow was driven by gravity. Another interesting experiment related to water exit was carried out by Reis et al. (2010) in order to investigate the cat-lapping phenomenon.

From the modelling point of view, most studies agree that water exit is not the time reversal of water entry. Chapman et al. (1997) and Gillow (1998) argue that, from the mathematical point of view, the solution of the Wagner problem is only stable for a wetted surface of increasing area. However, one can find several studies on water entry and exit based on the Wagner or the von Karman model (see Baarholm and Faltinsen, 2004; Bensch et al., 2001 for example). In these studies, the formula for the hydrodynamic force during the exit stage is obtained by modifying the formula derived for the entry stage. This idea was already used by Kaplan (1987), but it lacks clear justification.

In the following sections, we present a semi-analytical model of water entry and exit based on the MLM and the von Karman approach. The MLM has been extended to the water entry of a body whose shape varies in time, and is used for the entry stage. The original MLM was modified with the aim to match it with the model of water exit. A modified von Karman approach consistent with the MLM is proposed for the exit stage. In the proposed von Karman approach, the position of the contact point is given by the intersection between the body and a reference water level corresponding to the vertical position of the contact point at the transition between the entry and exit stages. The pressure is computed by the linearised Bernoulli equation and the time derivative of the velocity potential is determined by solving the boundary-value problem satisfied by the acceleration potential. It is shown that enforcing a Kutta condition at the contact point leads to the same formula as the one used by Kaplan (1987) for a rigid body. With the help of the acceleration potential, we avoid the difficult calculation of the velocity potential in the wake region. The presence of a wake region during the exit stage is responsible for the restriction of the Wagner model to the entry stage only. Several case studies are presented: the water entry and exit of a wedge, the water entry and exit of a parabola, and finally the water entry and exit of an expanding and contracting circular cylinder. Comparisons with CFD results are presented for each case in order to show the capabilities of the model.

The paper is arranged as follows. Section 2 introduces the analytical model of water entry and exit. Section 3 describes the CFD solver and its main characteristics. Results for rigid bodies and a body whose shape varies in time are discussed in Section 4. Conclusions are drawn in Section 5.

## 2. Analytical model of water entry and exit

In this section we describe a two-dimensional semi-analytical model of water entry and exit of a body whose shape is changing in time. The liquid is initially at rest and occupies the lower half plane ($z \le 0$). The $z$-axis points vertically up. The position of the body surface at time instant $t$, $t \ge 0$, is described by the equation $z = Zb(y,t)$, where $Zb$ is a given function such that $Zb(-y,t) = Zb(y,t)$ and $Zb(0,0) = 0$ (see Fig. 2). We assume $Zb(y,0) \ge 0$ so that the body lies above the waterline at time $t = 0$ of first contact. The region of contact between the body and the liquid corresponds to the interval $-c(t) < y < c(t)$. The water entry stage is defined as the time interval $[0,\ t_0]$ during which the wetted surface is expanding: $\dot{c}(t) \ge 0$, where the dot stands for the time derivative. During the exit stage, the wetted surface is contracting: $\dot{c}(t) < 0$ for $t > t_0$.

Similar to the asymptotic theory of water impact of rigid bodies, the water entry and exit problems are formulated using potential flow theory in which gravity, compressibility and viscosity are neglected. See Oliver (2002) for more details on the Wagner theory.

### 2.1. Water entry stage

This section describes the extension of the MLM to the water entry of a body whose shape varies in time. The main features of this model are the computations of the contact point position, the hydrodynamic pressure and the hydrodynamic force.

#### 2.1.1. Contact point position

Within the MLM as described by Korobkin (2004), the contact point position $y = c(t)$ is determined according to the Wagner condition. For a symmetric body, Korobkin (1996) showed that this condition can be written as

$$\int_0^{\pi/2} Zb[c(t)\ \sin\ \gamma, t]\,\mathrm{d}\gamma = 0, \quad t \le t_0. \tag{1}$$

Eq. (1) yields that $c(t)$ only depends on the current body position $Zb(y,t)$ and does not depend on the previous history of the body motions and body deformations. That is, there is no memory effect in this approach in terms of the size of the contact region. The derivative $\dot{c}(t)$ can be obtained by differentiating both sides of Eq. (1) with respect to $t$.

#### 2.1.2. Hydrodynamic pressure

Assuming zero atmospheric pressure at the free surface, the hydrodynamic pressure in the liquid domain is given by the nonlinear Bernoulli equation:

$$p(y,z,t) = -\rho(\varphi_t + \tfrac{1}{2}|\nabla\varphi|^2), \tag{2}$$

where $\varphi$ is the velocity potential, $\rho$ is the liquid density, $\varphi_t$ denotes the partial derivative of $\varphi$ with respect to $t$ and we use the subscripts notation to denote partial derivatives in the following equations. Note that $\varphi$ is governed by the Laplace equation in the fluid domain and satisfies the dynamic and kinematic boundary conditions on the free surface (a material boundary with zero pressure) and on the impermeable body contour. Following Korobkin (2004), we introduce

$$P(y,t) = p(y, Zb(y,t), t), \tag{3}$$

$$\phi(y,t) = \varphi(y, Zb(y,t), t), \tag{4}$$

which are the pressure and the velocity potential on the body surface $z = Zb(y,t)$. Using Eq. (4), the body boundary condition, $\varphi_z = Zb_t + Zb_y \cdot \varphi_y$, and substituting Eqs. (2) and (3) we find

$$P(y,t) = -\rho\left[\phi_t - \frac{Zb_t Zb_y}{1+(Zb_y)^2}\phi_y + \frac{1}{2}\frac{(\phi_y)^2 - (Zb_t)^2}{1+(Zb_y)^2}\right]. \tag{5}$$

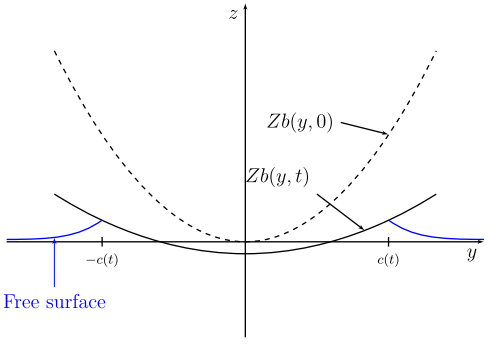


**Fig. 2.** Water entry of a body whose shape is changing in time.

Note that potential flow theory is the only assumption used to derive Eq. (5) and that $\varphi$ in (4) is the solution of the fully nonlinear boundary value problem governing the water impact (see Battistin and Iafrati, 2003 for details). Also note that the vertical water entry of a rigid body at constant speed $V$ studied in Korobkin (2004) corresponds to the case $Zb_t(y,t)=V$.

Subsequent approximations are introduced in the following steps. Within the MLM, the body potential $\phi$ is approximated by the velocity potential provided by the original Wagner model, $\varphi^{(w)}$, and a Taylor expansion of $\varphi^{(w)}$ about $z=0$:

$$\phi(y,t)\approx\varphi^{(w)}(y,Zb(y,t),t)\approx\varphi^{(w)}(y,0,t)+Zb(y,t)\cdot\varphi_z^{(w)}(y,0,t), \tag{6}$$

where $\varphi^{(w)}$ is the solution of the following linear boundary-value problem:

$$\varphi_{yy}^{(w)}+\varphi_{zz}^{(w)}=0 \quad (z<0), \tag{7a}$$

$$\varphi^{(w)}=0 \quad (z=0,|y|\geq c(t)), \tag{7b}$$

$$\varphi_z^{(w)}=Zb_t(y,t) \quad (z=0,|y|<c(t)), \tag{7c}$$

$$\varphi^{(w)}\to 0 \quad (y^2+z^2\to\infty). \tag{7d}$$

In Eqs. (7) the boundary conditions are imposed on the initial free surface level ($z=0$). The calculation of $\varphi^{(w)}$, and therefore the approximation of $\phi$, is much simpler than the computation of $\varphi$. Finally, substituting Eq. (6) into Eq. (5) gives us the pressure on the wetted part of the body:

$$P(y,t)=-\rho\left\{\varphi_t^{(w)}+\varphi_y^{(w)}\cdot\frac{Zb_{ty}\cdot Zb}{1+(Zb_y)^2}+\frac{[\varphi_y^{(w)}]^2}{2[1+(Zb_y)^2]}+\frac{(Zb_{ty})^2\cdot Zb^2}{2[1+(Zb_y)^2]}+Zb_{tt}\cdot Zb+\frac{1}{2}(Zb_t)^2\right\}, \tag{8}$$

where $\varphi_t^{(w)}(y,0,t)$ and $\varphi_y^{(w)}(y,0,t)$ are calculated at $z=0$ using the Wagner model (7). In Eq. (8) we have assumed that $Zb_{ty}=Zb_{yt}$ in the mixed partial derivatives of the given function $Zb(y,t)$. The velocity potential should be continuous on the liquid boundary $z=0$. The Wagner model gives (see Appendix A.1)

$$\varphi^{(w)}(y,0^-,t)=\frac{-I_1(y,t)}{\pi}\sqrt{c^2(t)-y^2}, \tag{9}$$

where $|y|<c(t)$ and $I_1(y,t)$ is defined by

$$I_1(y,t)=PV\int_0^c\frac{2\tau\theta(\tau,t)\,\mathrm{d}\tau}{(\tau^2-y^2)\sqrt{c^2(t)-\tau^2}}, \tag{10}$$

where $PV$ denotes a principal value integral. The function $\theta(y,t)$ in (10) is the stream function on the body surface, calculated by

$$\theta(y,t)=-\int_0^y Zb_t(\tau,t)\,\mathrm{d}\tau. \tag{11}$$

Note that for a rigid body penetrating water without changing its shape, we have $Zb_t(y,t)=V$ and $\theta(y,t)=-V\cdot y$. Then Eqs. (A.8) and (10) provide the well known result $\varphi^{(w)}(y,0^-,t)=V\sqrt{c^2-y^2}$ (Wagner, 1932) and the derivatives $\varphi_t^{(w)}(y,0^-,t)$ and $\varphi_y^{(w)}(y,0^-,t)$ required in (8) are easy to calculate. However, for a body whose shape is changing in time, the calculation of these derivatives is not straightforward. In order to avoid the difficulties associated with the differentiation of Eq. (9) with respect to $t$ and $y$, we formulate the corresponding boundary-value problems for these two derivatives, $\varphi_t^{(w)}(y,z,t)$ and $\varphi_y^{(w)}(y,z,t)$, and solve them by using a similar technique as in Appendix A.1.

Differentiating Eqs. (7) with respect to time, we derive the boundary-value problem for the time derivative $\varphi_t^{(w)}(y,z,t)$:

$$\frac{\partial^2\varphi_t^{(w)}}{\partial y^2}+\frac{\partial^2\varphi_t^{(w)}}{\partial z^2}=0 \quad (z<0), \tag{12a}$$

$$\varphi_t^{(w)}=0 \quad (z=0,|y|\geq c(t)), \tag{12b}$$

$$\varphi_{tz}^{(w)}=Zb_{tt}(y,t) \quad (z=0,|y|<c(t)), \tag{12c}$$

$$\varphi_t^{(w)}\to 0 \quad (y^2+z^2\to\infty). \tag{12d}$$

This problem is solved in Appendix A.2. Note that the function $\varphi_t^{(w)}$ is square-root singular at $y=\pm c(t)$. The solution at $z=0$ is

$$\varphi_t^{(w)}(y,0^-,t)=\frac{-[I_2(y,t)+\pi D_0]}{\pi\sqrt{c^2(t)-y^2}}, \quad |y|<c(t), \tag{13}$$

where

$$I_2(y,t) = PV \int_{-c(t))}^{c(t)} \frac{\theta_t(\tau,t)\sqrt{c^2(t)-\tau^2}}{\tau - y}\, \mathrm{d}\tau, \tag{14}$$

$$\theta_t(y,t) = -\int_0^y Zb_{tt}(\tau,t)\, \mathrm{d}\tau, \tag{15}$$

$$D_0 = \frac{\dot{c}(t)c(t)}{\pi} I_1(c(t),t) - \frac{1}{\pi} I_2(c(t),t). \tag{16}$$

Similarly, $\varphi_y^{(w)}$ is determined as the solution of the following mixed boundary-value problem:

$$\frac{\partial^2 \varphi_y^{(w)}}{\partial y^2} + \frac{\partial^2 \varphi_y^{(w)}}{\partial z^2} = 0 \quad (z<0), \tag{17a}$$

$$\varphi_y^{(w)} = 0 \quad (z=0, |y| \geq c(t)), \tag{17b}$$

$$\varphi_z^{(w)} = Zb_t(y,t) \quad (z=0, |y|<c(t)), \tag{17c}$$

$$\varphi_y^{(w)} \to 0 \quad (y^2+z^2 \to \infty). \tag{17d}$$

The solution of this problem is given in Appendix A.3. On the liquid boundary, we obtain

$$\varphi_y^{(w)}(y,0^-,t) = \frac{1}{\pi\sqrt{c^2(t)-y^2}} I_3(y,t), \quad |y|<c(t), \tag{18}$$

where we define

$$I_3(y,t) = 2y \cdot PV \int_0^{c(t)} \frac{Zb_t(\tau,t)\sqrt{c^2(t)-\tau^2}}{\tau^2 - y^2}\, \mathrm{d}\tau. \tag{19}$$

Substituting Eqs. (13) and (18) into (8) leads to

$$\begin{aligned} \frac{P(y,t)}{-\rho} = {} & \frac{1}{\pi\sqrt{c^2(t)-y^2}} \left[ -\dot{c}(t)c(t) I_1(c(t),t) + I_3(y,t) \cdot \frac{Zb_{ty} \cdot Zb}{1+(Zb_y)^2} \right] \\ & + \frac{1}{c^2(t)-y^2} \cdot \frac{[I_3(y,t)]^2}{2\pi^2[1+(Zb_y)^2]} + \frac{(Zb_t)^2}{2} + \frac{(Zb_{ty})^2 Zb^2}{2[1+(Zb_y)^2]} \\ & + Zb_{tt}Zb + \frac{1}{\pi\sqrt{c^2(t)-y^2}} [I_2(c(t),t) - I_2(y,t)]. \end{aligned} \tag{20}$$

Note that the pressure $P(y,t)$ can be decomposed into

$$P = P_v + P_a, \tag{21}$$

with $P_v$ depending only on the body velocity ($Zb_t$):

$$\begin{aligned} \frac{P_v(y,t)}{-\rho} = {} & \frac{1}{\pi\sqrt{c^2(t)-y^2}} \left[ -\dot{c}(t)c(t) I_1(c(t),t) + I_3(y,t) \cdot \frac{Zb_{ty} \cdot Zb}{1+(Zb_y)^2} \right] \\ & + \frac{1}{c^2(t)-y^2} \cdot \frac{[I_3(y,t)]^2}{2\pi^2[1+(Zb_y)^2]} + \frac{(Zb_t)^2}{2} + \frac{(Zb_{ty})^2 Zb^2}{2[1+(Zb_y)^2]}, \end{aligned} \tag{22}$$

and $P_a$ depending only on the body acceleration ($Zb_{tt}$). Here $P_a$ can be rearranged as follows:

$$\frac{P_a(y,t)}{-\rho} = Zb_{tt}Zb + \frac{I_4(y,t)}{\pi}\sqrt{c^2(t)-y^2}, \tag{23}$$

where we define

$$I_4(y,t) = PV \int_0^{c(t)} \frac{-2\tau\theta_t(\tau,t)}{(\tau^2-y^2)\sqrt{c^2(t)-\tau^2}}\, \mathrm{d}\tau. \tag{24}$$

In order to compute the pressure, one has to evaluate $I_1(c(t),t)$, $I_3(y,t)$ and $I_4(y,t)$ from Eqs. (10), (19) and (24). This involves the calculation of principal value integrals of the following form:

$$PV \int_0^{c(t)} \frac{f(\tau,t)}{(\tau^2-y^2)\sqrt{c^2(t)-\tau^2}}\, \mathrm{d}\tau, \tag{25}$$

where $f(y,t)$ is a function which satisfies Hölder's condition with respect to $y$. Using the theory of Cauchy principal value integrals (see Gakhov, 1966), the integral defined in Eq. (25) can be transformed into an improper integral of the form:

$$PV\int_0^{c(t)}\frac{f(\tau,t)}{(\tau^2-y^2)\sqrt{c^2(t)-\tau^2}}\,\mathrm{d}\tau=\int_0^{c(t)}\frac{f(\tau,t)-f(y,t)}{(\tau-y)(\tau+y)\sqrt{c^2(t)-\tau^2}}\,\mathrm{d}\tau. \tag{26}$$

The Hölder condition on $f$ ensures that the improper integral in the right-hand side of Eq. (26) converges.

#### 2.1.3. Hydrodynamic force

From Eq. (20), one can see that $P_v$ behaves asymptotically like

$$P_v(y,t)\sim\rho\frac{A(t)}{\sqrt{c^2(t)-y^2}}-\rho\frac{B(t)}{c^2(t)-y^2},\quad |y|\to c(t), \tag{27}$$

where $A(t)$ and $B(t)$ are positive. In the original Wagner model, $B(t)=0$ and the pressure tends to $+\infty$ but is integrable at $|y|=c(t)$. In the MLM, the positive peak pressure is finite in the neighbourhood of $|y|=c(t)$ as $[c^2(t)-y^2]^{-1}$ is a stronger singularity than $[c^2(t)-y^2]^{-1/2}$. However, near $|y|=c(t)$ the pressure is negative and not integrable, as $[c^2(t)-y^2]^{-1}$ is not integrable at $|y|=c(t)$. In Korobkin (2004), the hydrodynamic force is obtained by integrating the hydrodynamic pressure from $-c^*(t)$ to $c^*(t)$, the region of the wetted area where the pressure is positive, $c^*(t)$ being the closest point to $c(t)$ where $P_v(c^*(t),t)=0$. A similar process was first suggested by Zhao et al. (1997) for the integration of the pressure in the generalised Wagner model, judging that the negative pressures obtained close to $|y|=c(t)$ are unphysical. In both Korobkin (2004) and Zhao et al. (1997), it is assumed that the body is rigid and falling at constant speed or that $|Zb_t|\gg|Zb_{tt}|$ and therefore that: $P_v(c^*(t),t)=0$ implies $|P(c^*(t),t)|\ll 1$. In the present case of a body that enters and exits the water, just before the transition ($t=t_0^-$), the velocity of the body tends to 0 but the acceleration stays positive so we must find that $|Zb_{tt}|\gg|Zb_t|$. As a consequence, the pressure peak due to $P_v$ tends to 0 and $P_a$ becomes dominant. With $P_a<0$, the pressure might become negative all over the wetted surface, but $P_v$ remains non-integrable, even for small velocities. In order to deal with this issue, it is suggested to integrate the pressure in the following way to obtain the vertical hydrodynamic force $F$:

$$F(t)=\int_{-c^*(t)}^{c^*(t)}P_v(y,t)\,\mathrm{d}y+\int_{-c(t)}^{c(t)}P_a(y,t)\,\mathrm{d}y, \tag{28}$$

with $c^*(t)$ being the closest point to $c(t)$ where $P_v(c^*(t),t)=0$. For consistency with the exit model described in Section 2.2, we integrate $P_a$ over the entire wetted surface.

### 2.2. Water exit stage

In order to deal with the exit stage, a modified von Karman approach is proposed. The main features of this approach are the computations of the contact point position and the hydrodynamic pressure.

#### 2.2.1. Contact point position

Within the von Karman approach, the contact point position is determined as the geometric point of intersection between the initial water level and the body: $Zb(c(t),t)=0$. As this position is independent of the fluid flow, it can be also used during the exit stage. However, in order to enforce the continuity of the contact point position between the entry stage and the exit stage, the reference water level was modified, leading to the following condition:

$$Zb(c(t),t)=Zb(c(t_0),t_0),\quad t\geq t_0. \tag{29}$$

Note that this condition makes it also possible to take into account the rise of the free surface during the entry stage.

#### 2.2.2. Hydrodynamic pressure

Within the original von Karman approach, the pressure is given by the linearised Bernoulli equation:

$$P(y,t)=p(y,Zb(y,t),t)=-\rho\varphi_t^{(k)}(y,0,t), \tag{30}$$

where $\varphi^{(k)}$ is the velocity potential of the von Karman model during the exit stage. However, in order to be consistent with the entry stage and ensure a smooth transition, it is suggested to use the linearised equation (5) and a Taylor expansion with respect to $z$ of the acceleration potential similar to (6):

$$\phi_t(y,t)\approx\varphi_t^{(k)}(y,Zb(y,t),t)\approx\varphi_t^{(k)}(y,0,t)+Zb(y,t)\cdot\varphi_{tz}^{(k)}(y,0,t), \tag{31}$$

where $\varphi_{tz}^{(k)}(y,0,t)=Zb_{tt}(y,t)$. Altogether, this gives

$$P(y,t)=-\rho[Zb\cdot Zb_{tt}+\varphi_t^{(k)}(y,0,t)]. \tag{32}$$

It is therefore necessary to determine $\varphi_t^{(k)}$ during the exit stage. In order to do this, one may think of solving the problem for the velocity potential $\varphi^{(k)}$ and differentiating the result in time. However, during the exit stage, the velocity potential is the

solution of the following boundary value problem:

$$\varphi_{yy}^{(k)} + \varphi_{zz}^{(k)} = 0 \quad (z<0), \tag{33a}$$

$$\varphi^{(k)} = 0 \quad (z=0, |y| \geq c(t_0)), \tag{33b}$$

$$\varphi_t^{(k)} = 0 \quad \text{or} \quad \varphi^{(k)} = g(y) \quad (z=0, c(t) \leq |y| \leq c(t_0)), \tag{33c}$$

$$\lim_{|y|\to c(t)^-} |\varphi_t^{(k)}| < \infty \quad \text{or} \quad \lim_{|y|\to c(t)^-} |\varphi_y^{(k)}| < \infty \quad (z=0, |y|<c(t)), \tag{33d}$$

$$\varphi_z^{(k)} = Zb_t(y,t) \quad (z=0, |y|<c(t)), \tag{33e}$$

$$\varphi^{(k)} \to 0 \quad (y^2+z^2 \to \infty). \tag{33f}$$

The boundary condition (33c) is valid in the wake region of the free surface ($z=0, c(t) \leq |y| \leq c(t_0)$). But the function $g(y)$ in the wake region has to be determined together with the velocity potential. As no splash jet is forming during the exit stage, a Kutta condition must be satisfied at $|y|=c(t)$ to model the flow separation. A similar problem arises during the water impact of a flat plate at high horizontal speed (see Reinhard et al., 2011) where a Kutta condition is imposed at the trailing edge to model the flow separation. Note that Baarholm and Faltinsen (2004) simulated water impacts underneath horizontal decks using a boundary element model and "imposing a condition that requires the velocity potential to be continuous and the flow to be horizontal" at the separation point during the exit stage. One can see from Eq. (33c) that the boundary condition satisfied in the wake region by $\varphi_t^{(k)}$ is similar to the boundary condition satisfied in Eq. (12b) on the free surface. The acceleration potential is therefore the solution of the following boundary value problem:

$$\frac{\partial^2 \varphi_t^{(k)}}{\partial y^2} + \frac{\partial^2 \varphi_t^{(k)}}{\partial z^2} = 0 \quad (z<0), \tag{34a}$$

$$\varphi_t^{(k)} = 0 \quad (z=0, |y| \geq c(t)), \tag{34b}$$

$$\lim_{|y|\to c(t)^-} |\varphi_t^{(k)}| < \infty \quad (z=0, |y|<c(t)), \tag{34c}$$

$$\varphi_{tz}^{(k)} = Zb_{tt}(y,t) \quad (z=0, |y|<c(t)), \tag{34d}$$

$$\varphi_t^{(k)} \to 0 \quad (y^2+z^2 \to \infty). \tag{34e}$$

From Appendix A.2, the solution of Eqs. (34) is of the form

$$\varphi_t^{(k)}(y,0^-,t) = \frac{-[I_2(y,t) + \pi E_0]}{\pi\sqrt{c^2(t)-y^2}}, \quad |y|<c(t), \tag{35}$$

where $E_0$ is a real constant to be determined using the Kutta condition (34c):

$$E_0 = -I_2(c(t),t)/\pi. \tag{36}$$

Substituting $E_0$ into Eq. (35) and rearranging leads to

$$\varphi_t^{(k)}(y,0^-,t) = \frac{I_4(y,t)}{\pi}\sqrt{c^2(t)-y^2}, \quad |y|<c(t), \tag{37}$$

where $I_4(y,t)$ is defined in Eq. (24). The vertical component of the force is finally obtained by integrating the hydrodynamic pressure over the wetted surface:

$$F(t) = -\rho \int_{-c(t)}^{c(t)} \left[ Zb(y,t)\cdot Zb_{tt}(y,t) + \frac{I_4(y,t)}{\pi}\sqrt{c^2(t)-y^2} \right] \mathrm{d}y, \tag{38}$$

which is identical to integrating $P_a(y,t)$ over the wetted surface (see Eq. (23)). In this approach, the force depends on the acceleration only and not on the velocity of the body during the exit stage.

### 2.2.3. Discussion and comparison with previous work

In order to compare the approach described above with the approach used by Kaplan (1987) and others afterwards (see Baarholm and Faltinsen, 2004 for example), let us assume that the velocity and the acceleration of the wetted surface are uniform in space: $Zb_t(y,t) = V(t)$ and $Zb_{tt}(y,t) = \dot{V}(t)$. If no distinction is made between the entry stage and the exit stage (i.e. if one considers that the velocity potential is governed by Eqs. (7) instead of Eqs. (33) during both the entry and the exit stages), then the original Wagner theory leads to the following well known formula:

$$F(t) = -\rho\frac{\pi}{2}\dot{V}(t)c^2(t) - \rho\pi V(t)\dot{c}(t)c(t), \tag{39}$$

where the term proportional to $\dot{V}(t)$ is the so-called added mass term and the term proportional to $V(t)$ is commonly called the slamming term. During the entry stage, the body goes down ($V<0$) and the wetted surface is expanding: $\dot{c}(t)\geq 0$. During the exit stage, the body goes up ($V>0$) and the wetted surface is contracting: $\dot{c}(t)<0$. So the contribution of the slamming term to the force is always positive (i.e. directed upwards). In the work of Kaplan, the slamming term is suppressed in the exit stage. In fact, one can read in Kaplan (1992) that "this treatment is based on considerations of vertical momentum transfer only upon water entry and not during conditions associated with water exit". Although a similar justification can be found in other papers, such as Bensch et al. (2001), this process still lacks a clear justification. One possible explanation of the origin of this process might be that large upward forces were obtained from Eq. (39) during the exit stage, and were judged unphysical as they might have been in contradiction with experimental measurements. The remedy would therefore have been to keep only the added mass term which has a downward contribution to the force during exit. However, it is interesting to point out that the introduction of a Kutta condition as suggested in Eqs. (34), widely used to model flow separation, leads to the same result as the formula of Kaplan for exit. This can be checked by substituting $V$ and $\dot{V}$ into Eq. (38) and by neglecting the term $Zb\cdot Zb_{tt}$, which comes from the MLM formulation. This could therefore indicate that Eqs. (7) were used instead of Eqs. (33) when computing the velocity potential during the exit stage and that Eq. (39) was modified in order to be consistent with experimental results.

One can see that the force strongly depends on the contact point position $c(t)$. Therefore, Eq. (38) might give an accurate prediction of the force provided that the contact point position is known. As explained in Section 2.2.2, the velocity potential is the solution of Eqs. (33) during the exit stage and, as a consequence, the Wagner condition (1) is not valid during the exit stage. For this reason, it is suggested to use a von Karman-type condition for the computation of the contact point position (29). However, it is well known from studies on water entry that the von Karman condition does not provide an accurate prediction of the contact point position. Indeed, Wagner showed that accounting for the elevation of the free surface was important to accurately predict the contact position. Important improvement would probably be provided to the model by taking into account the fluid flow for the computation of the contact point position. Unfortunately, we have not found a condition equivalent to the Wagner condition for the exit stage.

### 2.3. Implementation of the analytical model

The construction of an analytical solution based on the model described in Sections 2.1 and 2.2 involves the following subsequent steps:

(a) the computation of the contact point position,
(b) the computation of the time-derivative of the contact point position during the entry stage,
(c) the computation of the hydrodynamic pressure,
(d) the computation of the hydrodynamic force by integrating the hydrodynamic pressure.

Note that the contact point position $c(t)$ is determined from Eq. (1) and the time derivative of the contact point position $\dot{c}(t)$ is obtained by substituting the value of $c(t)$ previously calculated into the time-derivative of Eq. (1) during the entry stage. As soon as $\dot{c}(t)$ becomes negative, the exit stage starts and the contact point position is computed using Eq. (29). For this purpose, the elevation of the free surface at the instant of transition, $Zb(c(t_0),t_0)$, has to be determined precisely. In order to study the water entry and exit of arbitrary shapes, we used a numerical procedure which assumes that the body surface is defined in a discretised form at a number of nodes, denoted $y^n$, and interpolated linearly between each node:

$$Zb(y,t)=\frac{Zb(y^{n+1},t)-Zb(y^n,t)}{y^{n+1}-y^n}\cdot(y-y^n)+Zb(y^n,t),\quad y^n\leq y\leq y^{n+1}. \tag{40}$$

With such a description, the speed and acceleration of the body surface also evolve linearly between each node. Substituting Eq. (40) into Eq. (1), the position of the contact point $c(t)$ is determined by the secant method during the entry stage. Note that the determination of $c(t)$ during the exit stage is trivial, as the shape is interpolated linearly. In Eqs. (22), (23), (32) and (37), the singular terms of the hydrodynamic pressure distribution are factorised, and the functions $I_3(y,t)$ and $I_4(y,t)$ defined in Eqs. (19) and (24) are well behaved with respect to $y$. Thanks to this formulation, we accurately approximate the pressure distribution using a linear interpolation of $I_3(y,t)$ and $I_4(y,t)$ between each node. For this purpose, $I_1(c(t),t)$, $I_3(y^n,t)$, $I_3(c(t),t)$ and $I_4(y^n,t)$ are computed by substituting the discretised form of the body position (40) and its derivatives into Eqs. (10), (19) and (24). Making use of the formula presented in Eq. (26), the quantities $I_1(c(t),t)$, $I_3(y^n,t)$, $I_3(c(t),t)$ and $I_4(y^n,t)$ are rearranged into terms which can be integrated in closed form, and terms which can be reduced to elliptic integrals, for which standard numerical procedures exist. The position of $c^*(t)$ is determined by the secant method using the values of $I_1(c(t),t)$, $I_3(y^n,t)$, $I_3(c(t),t)$ and $I_4(y^n,t)$ previously computed. During the entry stage, the force is obtained by integrating $P_v$ and $P_a$ in Eq. (28) analytically from node to node using the same linear interpolation of $I_3(y,t)$ and $I_4(y,t)$ between the nodes. During the exit stage, the hydrodynamic force is obtained by integrating $P_a$ in Eq. (38) in the same way.

The nodes were uniformly distributed along the $y$-axis for the case studies presented in Section 4, the distance between the nodes being 5 mm for the wedge and the parabola and $R(t_0)/500$ for the expanding and contracting cylinder.

## 3. CFD method

This section describes the Computational Fluid Dynamcis (CFD) methodology used to generate the reference results for the entry and exit cases studied in this paper. A custom solver built on the open-source finite-volume CFD library OpenFOAM® is used to numerically solve the Navier–Stokes equations governing the air–water flow. See Piro and Maki (2013b) for more details.

### 3.1. Governing equations

The arbitrary Lagrangian–Eulerian (ALE) form of the Navier–Stokes Equations is solved using the finite-volume technique (more details can be found from many sources, see Jasak, 2009 as an example). This approach allows for solution on moving and deforming meshes. The governing equations are given below:

$$\nabla \cdot \vec{u} = 0, \tag{41}$$

$$\frac{\partial \rho \vec{u}}{\partial t} + \nabla \cdot \rho \vec{u}(\vec{u} - \vec{u}_g) = -\nabla p + \nabla \cdot (\mu(\nabla \vec{u} + \nabla \vec{u}^{\top})), \tag{42}$$

where $\vec{u}$ is the fluid velocity, $\vec{u}_g$ is the grid velocity, $\rho$ and $\mu$ the fluid density and dynamic viscosity, and $p$ the fluid pressure. The results generated for this paper neglect gravity to be consistent with the analytical model that is presented in Section 2. Turbulence is also neglected in this work because the time scales of the current problems are too short for a turbulent flow to develop and influence the results. The values of $\mu$ used are $10^{-3}$ kg m$^{-1}$ s$^{-1}$ for water and $1.48 \times 10^{-5}$ kg m$^{-1}$ s$^{-1}$ for air, and the values of $\rho$ are 1000 kg m$^{-3}$ for water and 1 kg m$^{-3}$ for air.

The entry and exit of bluff and wedge-shaped bodies can generate complex free-surface topology. For example during entry a very thin jet emerges from a region where the pressure gradient is largest. To solve for the evolution of the fully nonlinear air–water interface, the volume-of-fluid (VOF) method is employed. Ubbink and Issa (1999) provide a good reference for the use of VOF on arbitrary unstructured finite-volume discretisation of the fluid domain. In this work a special advection equation is used that provides a sharp transition between the two phases. The advection equation governing the phase-indicator variable $\alpha$ is

$$\frac{\partial \alpha}{\partial t} + \nabla \cdot (\alpha \vec{u}) + \nabla \cdot (\alpha(1-\alpha)\vec{w}) = 0, \tag{43}$$

where $\alpha$ is the scalar indicator variable that takes a value between 0 and 1, 0 representing air and 1 is water. The last term in this equation uses a compressive velocity field $\vec{w}$ that is oriented normal to the air–water interface. The factor $\alpha(1-\alpha)$ is zero away from the interface. Details on the computation of $\vec{w}$ can be found in Piro and Maki (2013a). The solver used is the `interDyMFoam` solver in OpenFOAM version 2.1.1 modified to include the compression velocity of Piro and Maki (2013a).

### 3.2. Discretisation

The geometry and the fluid solution for the problems studied in this paper are symmetrical about the $y=0$ plane. The CFD simulations are performed on a fluid discretisation that encompasses one-half of the body and corresponding fluid domain. The discretisation of the fluid domain is generated with the `snappyHexMesh` utility available in the OpenFOAM® library. This utility takes a uniform background grid, removes the cells that are not in the fluid domain (i.e. inside the body), and refines the grid near the body and in any other user-specified region. This automatic process generates a mesh that is uniform everywhere except in the immediate neighbourhood of the body boundary, and in regions where there is a transition in the level of refinement. In this work, refinement is used in the region where the air–water interface passes.

Table 1 shows mesh characteristics for the three different cases in this paper. Specifically, the number of cells in the mesh and the length scale of the smallest cell relative to the body size are given. Also, Fig. 3 shows the mesh around the cylinder with a close-up near the body. The cylinder is the darker gray portion of the figure.

**Table 1**
Mesh characteristics for the three cases.

| Case | Number of cells | Minimum cell size |
|---|---|---|
| Wedge | 29 200 | $3.750 \times 10^{-4}B$ |
| Parabola | 1 013 760 | $6.313 \times 10^{-4}B$ |
| Cylinder ($k$=1.10,1.25) | 112 123 | $6.256 \times 10^{-3}R_0$ |
| Cylinder ($k$=1.025,1.05) | 1 635 109 | $1.563 \times 10^{-3}R_0$ |

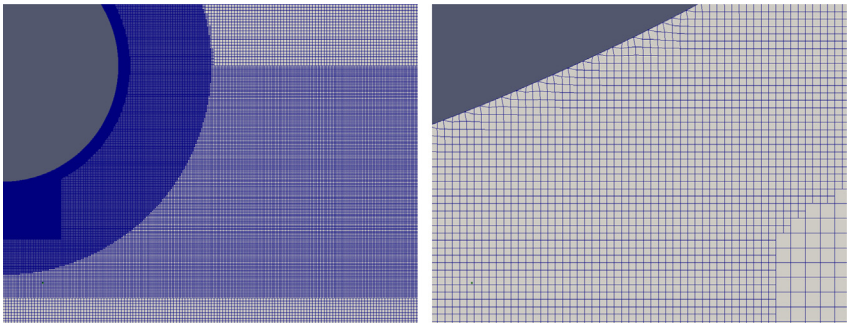

**Fig. 3.** View of the mesh used for the cylinder cases with refinement near the body (shown in gray). Picture on right shows a close-up of the mesh near the body.

The time step size is adaptively chosen during the simulations such that the maximum local Courant Number throughout the domain is less than 0.3. Typical time step sizes in this work range from $5.0 \times 10^{-5}$ to $10^{-3}$ s depending on the case and time within the simulation. Testing has been done with a constant time step size to ensure that the adaptive step size does not compromise the solution accuracy.

The spatial and temporal discretisations determine the amount of CPU time required to complete the CFD simulations. For the expanding and contracting cylinder, the required CPU time ranges from 4.8 h on 1 processor for $k=1.10$ (coarser mesh) to 82.7 h on 12 processors – 992.4 total CPU hours – for $k=1.05$ (finer mesh).

### 3.3. Dynamic mesh and boundary conditions

The entry and exit simulations use both the moving and deforming mesh strategies. Moving mesh denotes cases where the entire mesh is translated and rotated with the body motion. The entry and exit of both the wedge and parabola use the moving-mesh strategy.

The fluid grid points on the body boundary are moved with the body in the deforming mesh simulations. On all other boundaries, the grid points are static. The internal grid point motion is assumed to be governed by Laplace's equation. The deforming mesh strategy is used for the expanding and contracting circular cylinder simulations.

In both cases, the ALE equations (41) and (42) govern the solution of the velocity and pressure in an inertial reference frame. The grid moves relative to this inertial reference frame. In this frame, the body boundary condition is the fluid velocity equals the body velocity. The velocity at the bottom boundary is set to a fixed value of $\vec{0}$ in all cases. At the top boundary, the velocity is set to a zero-normal-gradient (or an outlet condition). The pressure boundary conditions are zero-normal-gradient on all boundaries except the top, where it is set to a fixed value of zero.

## 4. Results

This section presents results for several case studies of water entry and exit to which the analytical model is applicable. In addition, comparisons with CFD results are presented for several cases. The water entry and exit of a wedge, a parabola, and an expanding and contracting cylinder are considered. The wedge and the parabola are important cases for the assessment of the accuracy of the analytical model on simple cases for applications involving structures subject to water entry and exit such as ship structures or wave energy harvesting devices (see De Backer et al., 2010).

### 4.1. Water entry and exit of a wedge

Let us consider the water entry and exit of a rigid wedge with a deadrise angle $\beta$ of $10^\circ$ as considered in Piro and Maki (2011, 2013b). The body position is defined as $Zb(y,t)=|y|\cdot\tan\beta+Z(t)$, with $Z(t)=(V_1/2)t^2+V_0t$ and $\beta=10^\circ$. The initial velocity is $V_0=-4$ m s$^{-1}$ and $V_1$ is such that $Z(t_0)=-(B/4)\tan\beta$, where $B=1\cdot\cos\beta$ m is the total width of the wedge specimen and $t_0$ is the instant of transition between entry and exit ($t_0=-V_0/V_1$). Within these conditions, $V_1=2V_0^2/(B\tan\beta)$. Note that the chines of the wedge remain dry during entry and exit: $c(t)<B/2$. Fig. 4 depicts the nondimensional force $F^*=F/(\rho V_0^2 B)$ as a function of the nondimensional time $t^*=t/t_0$ during the water entry and exit of the wedge. One can see that the force is positive (directed upward) in the first part of the entry stage and that the force is negative afterwards. Indeed, the effect of acceleration/deceleration ($\ddot{Z}=V_1$), which is rather similar to the added mass effect, increases as the wetted area increases and that of the "slamming term" decreases as the velocity decreases (see Eq. (39)). It is remarkable that large downward forces appear during water entry ($t^*<1$). Moreover, the magnitude of the greatest downward force is greater than the maximum positive force. One can see that the results by the analytical model and CFD are in very good agreement during the entry stage and that the analytical model makes it possible to take into account the rise of the free surface during the exit stage:

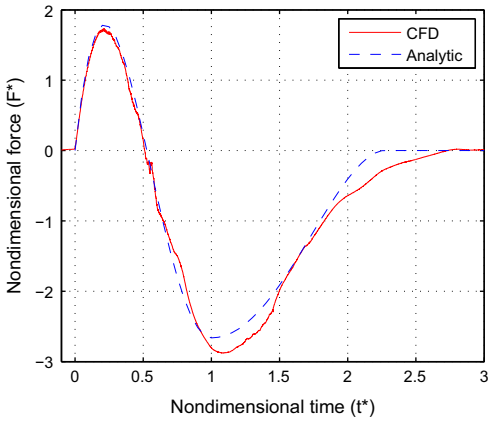


**Fig. 4.** Nondimensional force evolution as a function of the nondimensional time during the water entry and exit of a wedge.

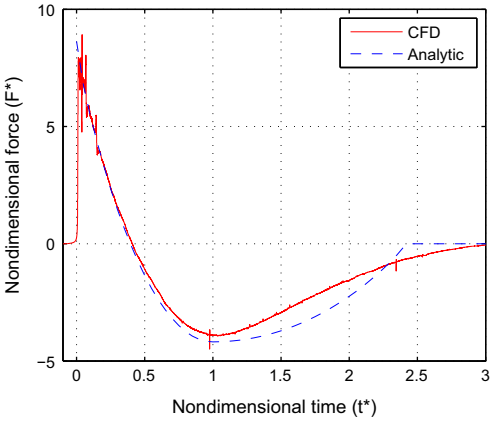


**Fig. 5.** Nondimensional force evolution as a function of the nondimensional time during the water entry and exit of a parabola.

$F^*(t^*=2)\neq 0$. In particular, the amplitude of both extreme forces predicted by the analytical model and by CFD are very close. However, the CFD simulation predicts a longer exit stage which is not as well captured by the analytical model.

### 4.2. Water entry and exit of a parabola

The water entry and exit of a rigid parabola is now considered. The body position is defined as $Zb(y,t)=y^2\cdot\tan(\beta)/B+Z(t)$, with $Z(t)=(V_1/2)t^2+V_0t$, $V_0=-1\ \mathrm{m\ s^{-1}}$, $V_1=19.5376\ \mathrm{m\ s^{-2}}$, $B=1\ \mathrm{m}$ and $\beta=20^\circ$. Note that with these parameters the maximum local deadrise angle at the contact point is about 15.2685 ° at $t^*=t/t_0=1$. The nondimensional force ($F^*=F/(\rho V_0^2B)$) is depicted in Fig. 5 as a function of the nondimensional time ($t^*$). Similar to the case of the wedge, the force becomes directed downward during the entry stage. However, the time evolution is different. In particular, in contrast to the wedge, one can see that the force predicted by the analytical model is non-zero at $t^*=0^+$ (the force obtained by the analytical model starts at $t=0^+$). This is a well known result of the original Wagner model, which is based on incompressible flow theory and gives a finite force at the first instant of point contact between a blunt body and the water surface. Indeed, within the Wagner theory the force is equal to $F_0=2\pi\rho V_0^2R$ at $t=0^+$, with $R$ the radius of curvature of the blunt body at $y=0$ and $V_0$ the velocity of the body at $t=0^+$. Although the MLM tends to the same limit at $t=0^+$, this limit cannot be reached by integrating the pressure distribution as described in Section 2.1.3, as the wetted area tends to a single point. However, the force can be extrapolated to the Wagner limit ($F_0$) at $t=0^+$. It is interesting to note that the acceleration has no effect on this limit as the added mass is zero when $c(t)=0$. The extreme negative forces predicted by both methods at $t^*=1$ (the time of deepest immersion) are very close to each other. In contrast to the wedge case study, for the parabola, the magnitude of the extreme downward force is smaller than the magnitude of the extreme upward force. This highlights an interesting difference between the water entry and exit of a blunt body and the water entry and exit of a wedge. The good agreement between the two approaches is confirmed by comparing the pressure coefficient distributions ($C_p=P/(0.5\rho V_0^2)$), which are plotted in Figs. 6 (entry stage) and 7 (exit stage). One can see that during the early stage of impact (Fig. 6(a)) the pressure coefficient is positive all over the wetted surface and that the pressure peak is well pronounced. Air is modelled in the CFD simulation, so the water surface is slightly deformed due to the air-flow and the force is non-zero just before $t^*=0$. As time increases, the amplitude of the pressure coefficient decreases and a region of negative

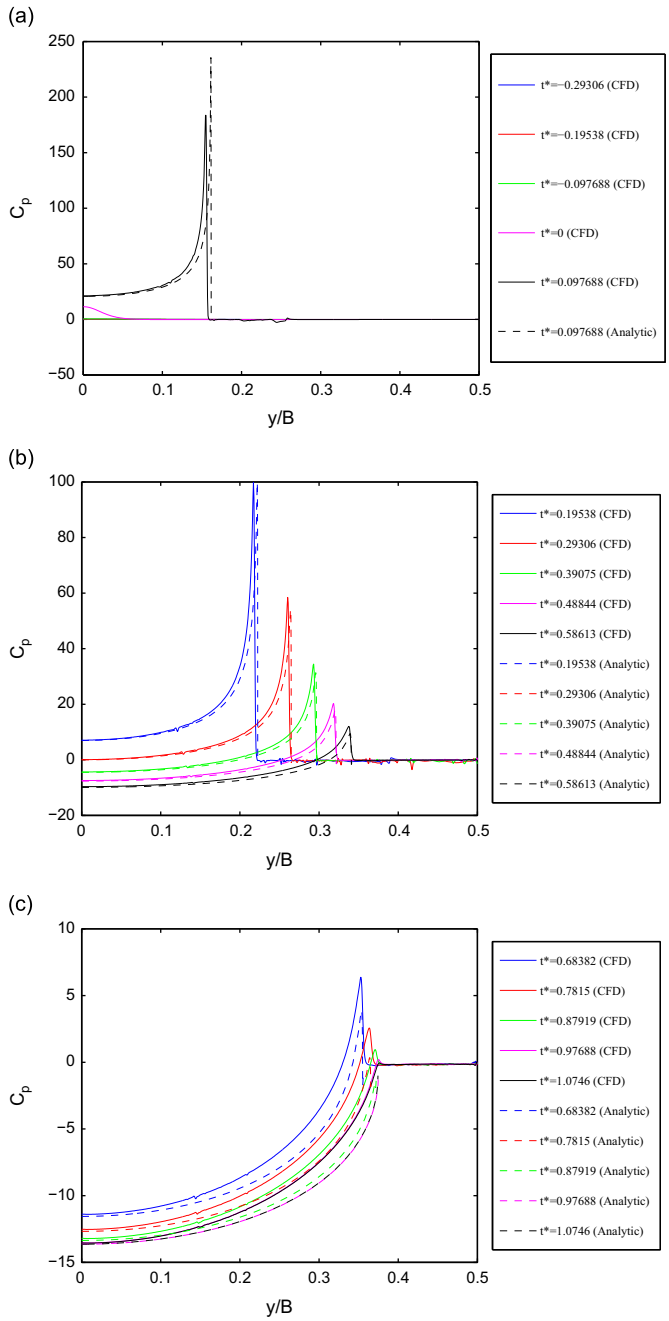


**Fig. 6.** Distribution of pressure coefficient $C_p$ as a function of $y/B$ at successive times during the water entry of a parabola: (a) from $t^* = -0.29306$ to $t^* = 0.097688$ (b) from $t^* = 0.19538$ to $t^* = 0.58613$ (c) from $t^* = 0.68382$ to $t^* = 1.0746$.

pressure coefficient appears in the centre of the wetted region (Fig. 6(b)). This is due to the decrease of the entry velocity and to the decrease of the local deadrise angle at the contact point. One can see in Fig. 6(c) that the pressure peak keeps on decreasing until it vanishes just before $t^*=1$. Note that at $t^* = 0.87919$, the pressure predicted by the MLM is already negative all over the wetted surface. After the transition, the pressure coefficient distributions obtained from the analytical model and the CFD simulation remain close to each other (Fig. 7(a)). In particular, one can see that the contact point position is well estimated by the modified von Karman approach. However, later in the exit stage, differences increase (Fig. 7(b)). Finally, one can see that both the magnitude of the pressure distribution and the position of the contact point are rather different when the parabola is about to leave the water (Fig. 7(c)). This last remark suggests that the prediction of the contact point position in the analytical model could be improved. Indeed, it is not surprising to see that, like the von Karman model for water entry, the von Karman model for exit also underestimates the wetted area. Furthermore, nonlinearities could also be expected to have an increasing influence on the

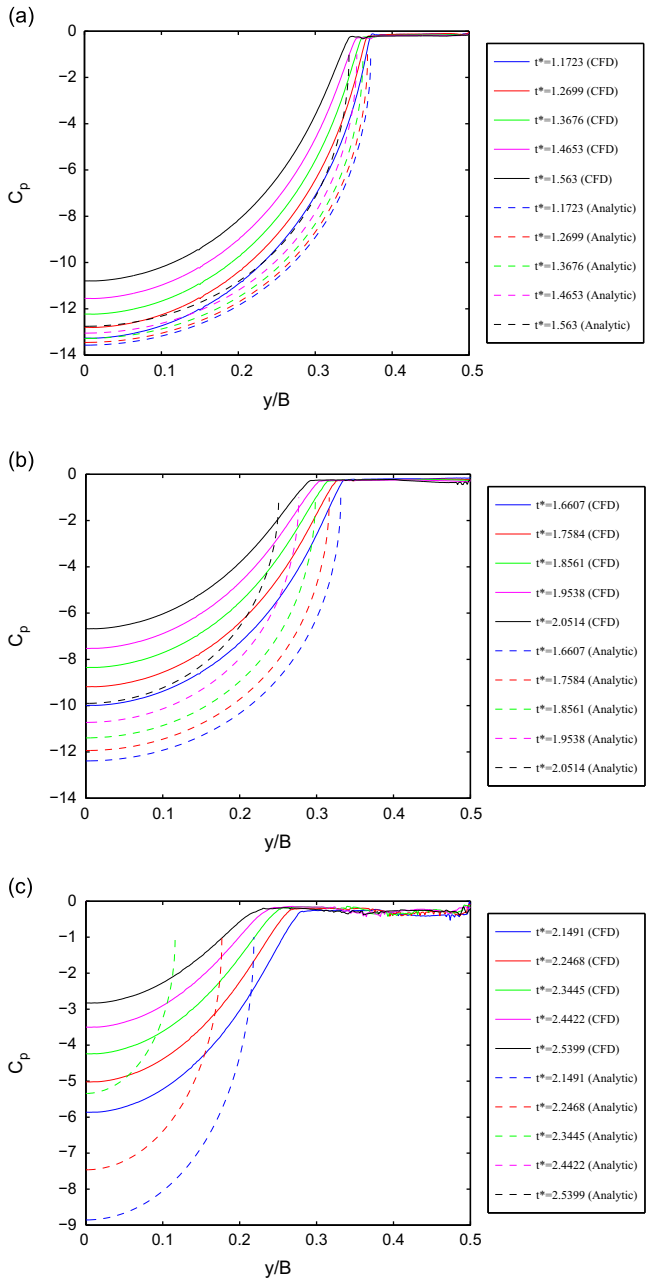


**Fig. 7.** Distribution of pressure coefficient $C_p$ as a function of $y/B$ at successive times during the water exit of a parabola: (a) from $t^* = 1.1723$ to $t^* = 1.563$; (b) from $t^* = 1.6607$ to $t^* = 2.0514$; (c) from $t^* = 2.1491$ to $t^* = 2.5399$.

pressure distribution as the velocity increases in the water exit stage. From the negative pressure coefficient distributions observed in Figs. 6 and 7, cavitation is likely to occur for high decelerations. As reported in Korobkin (2003) and Reinhard (2013), such decelerations could happen during the free-fall of a light-weight body impacting the water surface at high speed. This phenomenon would keep the pressure from dropping as low as predicted here and therefore limit the suction effect mentioned by Bensch et al. (2001) and Korobkin (2003).

### 4.3. *Water entry and exit of an expanding and contracting circular cylinder*

The water entry and exit of a circular cylinder initially laying in point contact with the water surface and whose radius increases and decreases is considered in this section. This problem comes from the $2D{+}t$ analysis of a curved body which moves horizontally at a fixed penetration depth (see Fig. 1). In such an analysis, the flow is studied in fixed vertical planes

which are "crossed" by the body (Fig. 1(a)). In the case of an ellipsoid of revolution, the three-dimensional problem is reduced to a sequence of two-dimensional problems which are similar to the water entry and exit of an expanding and contracting cylinder (Fig. 1(b)). In the present analysis, a slightly different case is considered in order to simplify the expression of the body position. Let the body position be defined as $Zb(y,t)=R_0-\sqrt{R(t)^2-y^2}$, with $R_0=0.65$ m and $R(t)=R_0+R_1t+R_2t^2$. Note that this case corresponds to the approximation of the ellipsoid shape by a panel of double curvature. The equivalent velocity $R_1$ and acceleration coefficient $R_2$ are determined such that the ratio of the maximum radius $R(t_0)$ of the cylinder to its initial radius $R_0$, $k=R(t_0)/R_0$, is respected. Several values of $k$ ranging from 1.025 to 1.25 are considered. Note that the position of the centre of the circular cylinder remains fixed at $z=R_0$ during entry and exit and that $R_1$ and $R_2$ are such that $t_0=0.5$ s in the simulations. In order to make a link between the results obtained and the well known results of the entry of a circular cylinder at constant speed and fixed radius, it is interesting to introduce a parameter $\zeta$ defined as $\zeta=-Zb(0,t_0)/R(t_0)=[R(t_0)-R_0]/R(t_0)$, which indicates the relative penetration depth at $t=t_0$. Here $\zeta$ indirectly gives information on the accuracy of the Wagner theory and the MLM during the entry stage, see Korobkin (2011). Note that $0.024\leq\zeta\leq0.2$ for the values of $k$ considered and therefore it is expected to be in the domain of validity of the Wagner theory. Fig. 8 depicts the evolution of the nondimensional force $F^*=F/(\rho R_1^2R_0)$ as a function of the nondimensional time $t^*$ for several values of the parameter $k$. One can see that the shape of the force curve is rather close to the one obtained for the parabola in Fig. 5. Indeed, these two body shapes are blunt and are expected to have similar behaviours. For both, the force starts impulsively and decreases until $t^*=1$. Note that the duration of negative force is also very long. During the entry stage, agreement between the two approaches is very close for all cases. For the $k=1.025$ case (Fig. 8(a)), the agreement during the exit stage is comparable to the one found for the parabola case. However, as the penetration parameter $k$ increases, the discrepancy increases significantly during the exit stage. It clearly appears that the analytical model overpredicts the magnitude of the negative force during the exit stage for the highest values of $k$. Note that for the greatest value of $k$ the local deadrise angle at the contact point reaches 55° at $t=t_0$ within the Wagner theory.

In Fig. 8(a) and (b) the force time series from the CFD simulations show high frequency oscillations, particularly during entry. This is due to the resolution of the pressure peak and jet root. The Courant number restriction limits the pressure

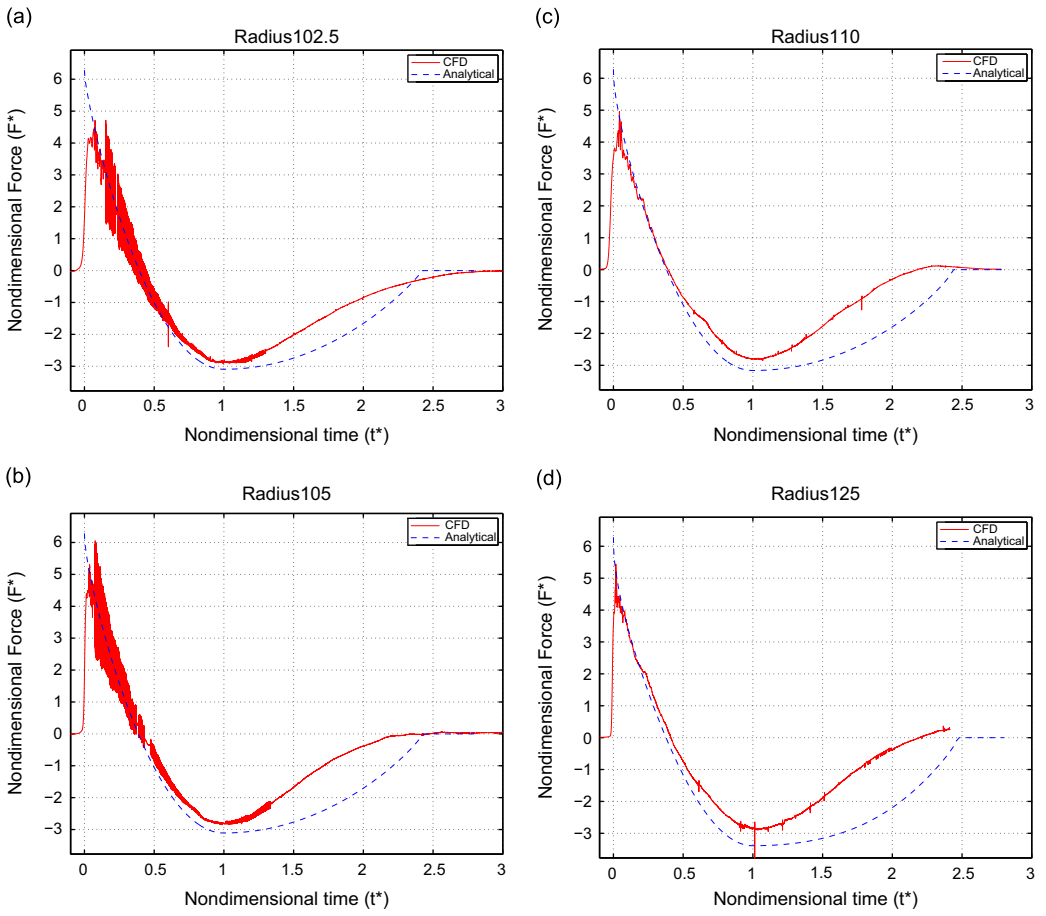


**Fig. 8.** Evolution of the nondimensional hydrodynamic force as a function of the nondimensional time during the water entry and exit of an expanding cylinder for several values of $k$.

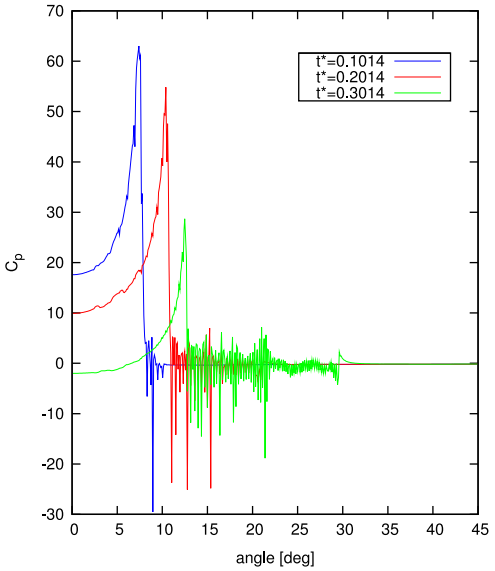


**Fig. 9.** Pressure coefficient $C_p = P/(0.5\rho R_1^2)$ as a function of the angle along the cylinder at three time instants for $k = 1.025$.

peak to moving approximately a third of a cell per time-step. The resolution of the peak thus changes in each time-step, depending on how close it is to a boundary face centre. This source of oscillation is magnified by finer grids since as the peak becomes more defined there is also a larger change in resolution. The second source of oscillation in the force time series is from the resolution of the jet root. The pressure profile of the $k = 1.025$ case is shown in Fig. 9 as a function of angular position, with $0^\circ$ corresponding to the centreline and $90^\circ$ a horizontal position. The figure shows that the pressure in the jet-root (angles just greater than that of the peak) is not smooth. As this jagged pressure profile moves along the body, oscillations are seen in the total force.

## 5. Conclusion

In this paper, an analytical model suitable to describe the water entry and exit of a body whose shape varies in time is proposed. This model is based on the modified Logvinovich model (MLM) for the entry stage. An extension of the MLM to bodies of varying shapes has been suggested for this purpose. A linear model of water exit based on the fundamental concepts of the von Karman model of water entry is proposed. In the present model, the method employed for the computation of the contact point position is modified in order to account for the rise of the free surface during entry. In order to compute the pressure, the acceleration potential is introduced and a Kutta condition is enforced at the contact point. It is shown that the present methodology leads to a formulation similar to the one used by Kaplan (1987). Explicit formulae are derived for the computation of the derivatives of the velocity potential of Wagner using the theory of analytic functions and introducing the acceleration potential and the complex velocity. The analytical model has been used to study the water entry and exit of rigid bodies and bodies whose shapes vary in time. In addition, CFD simulations have been run in order to provide reference results to the case studies considered. It is shown that important suction forces occur during the entry and exit stages. Although the exit model seems simple, it makes it possible to provide rational force predictions where the Wagner theory ceases to be valid. The model provides good results for bodies with small deadrise angles. However, when large penetration depths and large deadrise angles are concerned, some clear limitations arise. This work shows the possibility to predict accurately the suction effects during the water entry and exit. The results obtained from the analytical model presented in Section 4.2 show that the absolute hydrodynamic pressure is likely to drop below the vapour pressure of the liquid for large decelerations. In that sense, the model can be used to predict the onset of cavitation, which would have a limiting effect on downward forces. Furthermore, in the light of the expanding and contracting cylinder studied in Section 4.3, this model can be used to study hydroelastic problems involving water entry and exit. Repeated water entry and exit, such as an oscillating floating body, would however require a special treatment. Indeed, in the present state of the model, a cumulative rise of the reference water level would appear in that case.

Significant effort should be dedicated to the derivation of a better formulated exit model equivalent to the Wagner model of water entry. The results presented in Section 4 suggest that both the computation of the contact point position and of the pressure distribution could be improved. We suspect that the nonlinear terms of the Bernoulli equation might affect the pressure condition in the wake region. The notion of “contact point” itself, which is well established in the water entry theory (as there is a turnover region), might be less clearly defined in the exit stage because the water surface detaches smoothly from the solid surface.

Experimental investigations seem to be unavoidable in order to confirm the phenomena. For this purpose, one may be interested in performing water entry and exit experiments of the rigid bodies considered in Sections 4.1 (wedge) and 4.2 (parabola). In order to reproduce the conditions assumed in the analytical model (gravity neglected), the experimental conditions have to be such that $|V_1| \gg |g|$ ($g$ being the gravity acceleration here) and that the parameter $(V_0)^2/(BV_1)$ has the same value when comparing two cases. Reproducing experimentally the water entry and exit of the expanding and contracting cylinder is more challenging. One could imagine a device with several actuators able to bend a plate with the right shape.

## Acknowledgement

The work by Alan Tassin, Alexander A. Korobkin and Mark J. Cooker is part of the SMAES project which receives funding from the European Community's Seventh Framework Programme under grant agreement number FP7-266172. The effort of Dominic Piro and Kevin Maki is supported by the United States Office of Naval Research, under Grant numbers N00014-10-1-0301 and N00014-11-1-0846.

## Appendix A. Solutions of the mixed boundary value problems

This appendix details the derivation of the solutions of the mixed boundary value problems (7), (12) and (17) using the complex potential theory and the theory of analytic functions.

### A.1. Calculation of the velocity potential

The mixed boundary value problem defined in Eqs. (7) can be solved by introducing the analytic function $\Phi$ defined in $z<0$ as

$$\Phi(\xi) = [\varphi^{(w)}(y,z,t) + i\psi(y,z,t)]\sqrt{\xi^2 - c^2(t)}, \tag{A.1}$$

where the complex variable $\xi = y + iz$ and $\psi$ is the stream function ($\varphi^{(w)}_y = \psi_z$, $\varphi^{(w)}_z = -\psi_y$). Also note that $t$ appears as a parameter in Eqs. (7) and therefore in the function $\Phi$.

Using the following formulas:

$$\sqrt{\xi^2 - c^2} = -\sqrt{y^2 - c^2} \quad (y < -c, z = 0), \tag{A.2a}$$

$$\sqrt{\xi^2 - c^2} = \sqrt{y^2 - c^2} \quad (y > c, z = 0), \tag{A.2b}$$

$$\sqrt{\xi^2 - c^2} = -i\sqrt{c^2 - y^2} \quad (|y| < c, z = 0^-), \tag{A.2c}$$

one can show that the real part of $\Phi$ on the real-axis is given as follows:

$$\Re[\Phi(y + i0^-)] = 0, \quad |y| > c(t), \tag{A.3a}$$

$$\Re[\Phi(y + i0^-)] = \theta(y,t)\sqrt{c^2(t) - y^2}, \quad |y| < c(t), \tag{A.3b}$$

where $\theta(y,t) = \psi(y,0,t) = -\int_0^y Zb_t(\tau,t)\,\mathrm{d}\tau$ is the stream function on the wetted surface ($|y| < c$). The latter formula for the stream function along the wetted part of the body surface is also valid for the original nonlinear problem of symmetric body impact. Note that $\lim_{|\xi|\to\infty}\Phi(\xi) = iC_0$, with $C_0$ a real constant to be determined ($0 \le C_0 < +\infty$), so the solution of the Dirichlet problem (A.3) in the lower half-plane ($z<0$) is

$$\Phi(\xi) = \frac{i}{\pi}\int_{-\infty}^{+\infty} \frac{\Re[F(\tau + i0^-)]}{\tau - \xi}\,\mathrm{d}\tau + iC_0 = \frac{i}{\pi}\int_{-c(t)}^{c(t)} \frac{\theta(\tau,t)\sqrt{c^2(t) - \tau^2}}{\tau - \xi}\,\mathrm{d}\tau + iC_0. \tag{A.4}$$

From Sokhotsky–Plemelj's formula:

$$\lim_{\xi \to y + i0^-} \frac{i}{\pi}\int_{-c(t)}^{c(t)} \frac{\theta(\tau,t)\sqrt{c^2(t) - \tau^2}}{\tau - \xi}\,\mathrm{d}\tau = \theta(y,t)\sqrt{c^2(t) - y^2} + \frac{i}{\pi} PV \int_{-c(t)}^{c(t)} \frac{\theta(\tau,t)\sqrt{c^2(t) - \tau^2}}{\tau - y}\,\mathrm{d}\tau, \tag{A.5}$$

where $PV$ denotes the Cauchy principal value of the integral. Taking the imaginary part of $\Phi$ on the real-axis by using Eq. (A.5) and the definition of $\Phi$ leads to

$$\Im[\Phi(y + i0^-)]|_{|y|<c} = \frac{1}{\pi} PV \int_{-c(t)}^{c(t)} \frac{\theta(\tau,t)\sqrt{c^2(t) - \tau^2}}{\tau - y}\,\mathrm{d}\tau + C_0 = -\varphi^{(w)}(y, 0^-, t)\sqrt{c^2(t) - y^2}. \tag{A.6}$$

Enforcing the continuity of $\varphi^{(w)}(y, 0^-, t)$ at $y = c(t)$ leads to the following condition:

$$C_0 = -\frac{1}{\pi} PV \int_{-c(t)}^{c(t)} \frac{\theta(\tau,t)\sqrt{c^2(t)-\tau^2}}{\tau - c(t)}\, \mathrm{d}\tau. \tag{A.7}$$

Note that this condition is necessary to ensure that the kinetic energy is bounded in the fluid domain. Substituting Eq. (A.7) into Eq. (A.6) and rearranging leads to

$$\varphi^{(w)}(y,0^-,t) = \frac{-\sqrt{c^2(t)-y^2}}{\pi} I_1(y,t), \quad |y| < c(t), \tag{A.8}$$

where

$$I_1(y,t) = PV \int_0^{c(t)} \frac{2\tau\theta(\tau,t)\,\mathrm{d}\tau}{(\tau^2-y^2)\sqrt{c^2(t)-\tau^2}}. \tag{A.9}$$

### A.2. Calculation of the acceleration potential

The procedure described in Appendix A.1 can be used to find a solution of the boundary value problem defined in Eqs. (12). Let us introduce the analytic function $\Phi_t$ defined as

$$\Phi_t(\xi) = [\varphi_t^{(w)}(y,z,t) + i\psi_t(y,z,t)]\sqrt{\xi^2 - c^2(t)}, \tag{A.10}$$

where $\psi_t$ is the time derivative of the stream function $\psi$ ($\varphi_{ty}^{(w)} = \psi_{tz}$, $\varphi_{tz}^{(w)} = -\psi_{ty}$). One can show that

$$\Re[\Phi_t(y + i0^-)] = 0, \quad |y| > c(t), \tag{A.11a}$$

$$\Re[\Phi_t(y + i0^-)] = \theta_t(y,t)\sqrt{c^2(t)-y^2}, \quad |y| < c(t), \tag{A.11b}$$

where $\theta_t(y,t)$ is the partial $t$-derivative of $\theta(y,t)$. Note that $\lim_{|\xi|\to\infty}\Phi_t(\xi) = iD_0$, with $D_0$ a real constant to be determined ($0 \le D_0 < +\infty$). So by replacing subsequently $\Phi$, $\varphi^{(w)}$, $C_0$ and $\theta$ by $\Phi_t$, $\varphi_t^{(w)}$, $D_0$, and $\theta_t$, respectively, in Eqs. (A.4)–(A.6), one gets

$$\varphi_t^{(w)}(y,0^-,t) = \frac{-[I_2(y,t) + \pi D_0]}{\pi\sqrt{c^2(t)-y^2}}, \quad |y| < c(t), \tag{A.12}$$

where $I_2(y,t) = PV \int_{-c(t))}^{c(t)} (\theta_t(\tau,t)\sqrt{c^2(t)-\tau^2}/(\tau - y))\,\mathrm{d}\tau$ and $D_0$ is a constant to be determined. One can see that the constant $D_0$ governs the asymptotic behaviour of $\varphi_t(y,0^-,t)$ at $y = c(t)$ in Eq. (A.12):

$$\varphi_t^{(w)}(y,0^-,t) \sim \frac{-[I_2(c(t),t) + \pi D_0]}{\pi\sqrt{c^2(t)-y^2}} \quad \text{as } |y| \to c(t)^-. \tag{A.13}$$

In contrast to the velocity potential, the constant $D_0$ is determined by enforcing the asymptotic behaviour of Eq. (A.12) at $|y| = c(t)$ to be the same as the asymptotic behaviour of the time-derivative of Eq. (A.8). Differentiating Eq. (A.8) leads to

$$\frac{\partial\varphi^{(w)}}{\partial t}(y,0^-,t) = \frac{-\dot{c}(t)c(t)}{\pi\sqrt{c^2(t)-y^2}} I_1(y,t) - \frac{\sqrt{c^2(t)-y^2}}{\pi} \cdot \frac{\partial I_1(y,t)}{\partial t} \sim \frac{-\dot{c}(t)c(t)}{\pi\sqrt{c^2(t)-y^2}} I_1(c(t),t) \quad \text{as } |y| \to c(t)^-. \tag{A.14}$$

Equating Eqs. (A.(13) and A.14) leads to

$$D_0 = \frac{\dot{c}(t)c(t)}{\pi} I_1(c(t),t) - \frac{1}{\pi} I_2(c(t),t). \tag{A.15}$$

### A.3. Calculation of the velocity

In order to determine a solution of the mixed boundary value problem defined in Eqs. (17), the following analytic function $W$ is introduced:

$$W(\xi) = [\varphi_y^{(w)}(y,z) - i\varphi_z^{(w)}(y,z)]\sqrt{\xi^2 - c^2(t)}. \tag{A.16}$$

The real part of $W$ on the real-axis reads

$$\Re[W(y + i0^-)] = 0, \quad |y| > c(t), \tag{A.17a}$$

$$\Re[W(y + i0^-)] = -Zb_t(y,t)\sqrt{c^2(t)-y^2}, \quad |y| < c(t). \tag{A.17b}$$

Note that $\varphi_y^{(w)} = O((y^2+z^2)^{-1})$ as $|y^2+z^2| \to \infty$ and $|W(\xi)| \to 0$ as $|\xi| \to \infty$. Therefore $W$ is given by

$$W(\xi)=\frac{i}{\pi}\int_{-c(t)}^{c(t)}\frac{-Zb_t(\tau,t)\sqrt{c^2(t)-\tau^2}}{\tau-\xi}\,\mathrm{d}\tau. \tag{A.18}$$

From Sokhotsky–Plemelj's formula:

$$W(y+i0^-)=-Zb_t(y,t)\sqrt{c^2(t)-y^2}+\frac{i}{\pi}PV\int_{-c(t)}^{c(t)}\frac{-Zb_t(\tau,t)\sqrt{c^2(t)-\tau^2}}{\tau-y}\,\mathrm{d}\tau. \tag{A.19}$$

Therefore

$$\varphi_y(y,0^-)=\Re\left[\frac{W(y+i0^-)}{-i\sqrt{c^2(t)-y^2}}\right]=\frac{1}{\pi\sqrt{c^2(t)-y^2}}I_3(y,t),\quad |y|<c(t), \tag{A.20}$$

where $I_3(y,t)$ can be rearranged as follows:

$$I_3(y,t)=2yPV\int_0^{c(t)}\frac{Zb_t(\tau,t)\sqrt{c^2(t)-\tau^2}}{\tau^2-y^2}\,\mathrm{d}\tau. \tag{A.21}$$

## References


Aquelet, N., Souli, M., Olovsson, L., 2006. Euler–Lagrange coupling with damping effects: application to slamming problems. Computer Methods in Applied Mechanics and Engineering 195 (1–3), 110–132.

Baarholm, R., Faltinsen, O.M., 2004. Wave impact underneath horizontal decks. Journal of Marine Science Technology 9, 1–13.

Battistin, D., Iafrati, A., 2003. Hydrodynamic loads during water entry of two-dimensional and axisymmetric bodies. Journal of Fluids and Structures 17, 643–664.

Bensch, L., Shigunov, V., Beuck, G., Söding, H., 2001. Planned ditching simulation of a transport airplane. In: Krash Users Seminar, 7–10 January 2001, Tempe, AZ.

Chapman, S., Gillow, K., Howison, S., Ockendon, J., 1997. Asymptotics of violent surface motion. Philosophical Transactions of the Royal Society A 355, 679–685.

Climent, H., Benitez, L., Rosich, F., Rueda, F., Pentecote, N., 2006. Aircraft ditching numerical simulation. In: 25th International Congress of the Aeronautical Sciences—ICAS, 3–8 September 2006, Hamburg, Germany.

Cointe, R., Armand, J.-L., 1987. Hydrodynamic impact analysis of a cylinder. Journal of Offshore Mechanics and Arctic Engineering 109, 237–243.

De Backer, G., Vantorre, M., Frigaard, P., Beels, C., De Rouck, J., 2010. Bottom slamming on heaving point absorber wave energy devices. Journal of Marine Science and Technology 15 (2), 119–130.

Duez, C., Ybert, C., Barentin, C., Cottin-Bizonne, C., Bocquet, L., 2008. Dynamics of fakir liquids: from slip to splash. Journal of Adhesion Science and Technology 22, 335–351.

El Malki Alaoui, A., Nême, A., Tassin, A., Jacques, N., 2012. Experimental study of slamming coefficients during vertical water entry of axisymmetric rigid shapes at constant speeds. Applied Ocean Research 37, 183–197.

Faltinsen, O.M., Landrini, M., Greco, M., 2004. Slamming in marine applications. Journal of Engineering Mathematics 48, 187–217.

Faltinsen, O.M., Timokha, A.N., 2009. Sloshing. Cambridge University Press.

Gakhov, F., 1966. Boundary Value Problems. Nauka, Moscow (1977; English transl. of 2nd ed., Pergamon Press, Oxford, and Addison-Wesley, Reading, MA).

Gazzola, T., 2007. Contributions aux problèmes d'impacts non-linéaires : le problème de Wagner couplé. Ph.D. Thesis, Ecole Centrale Paris, France.

Gazzola, T., de Lauzon, J., 2008. Three-dimensional hydro-elastic Wagner impact using variational inequalities. In: 8th International Conference on Hydrodynamics, 30 September–3 October 2008, Nantes, France.

Gillow, K., 1998. Codimension-two Free Boundary Problems. D.Phil. Thesis, St Catherine's College, University of Oxford, UK.

Gong, K., Liu, H., Wang, B.-L., 2009. Water entry of a wedge based on SPH model with an improved boundary treatment. Journal of Hydrodynamics 21 (6), 750–757.

Greenhow, M., 1987. Wedge entry into initially calm water. Applied Ocean Research 9 (4), 214–223.

Greenhow, M., 1988. Water-entry and -exit of a horizontal circular cylinder. Applied Ocean Research 10 (4), 191–198.

Haboussa, G., Ortiz, R., Deletombe, E., Drazétic, P., 2008. A measurement study of a pressure transducer subjected to water drop impact. International Journal of Crashworthiness 13 (1), 49–66.

Hicks, P., Smith, F., 2011. Skimming impacts and rebounds on shallow liquid layers. Proceedings of the Royal Society A 467, 653–674.

Howison, S.D., Ockendon, J.R., Wilson, S.K., 1991. Incompressible water-entry problems at small deadrise angles. Journal of Fluid Mechanics 222, 215–230.

Iafrati, A., Broglia, R., 2008. Hydrodynamics of planing hulls: a comparison between RANS and 2*D*+*t* potential flow models. In: 27th Symposium on Naval Hydrodynamics, 5–10 October 2008, Seoul, Korea, pp. 795–813.

Jasak, H., 2009. Dynamic mesh handling in openfoam. In: 47th AIAA Aerospace Sciences Meeting, January 2009, Orlando, FL, USA.

Kaminski, M.L., Bogaert, H., 2009. Full scale sloshing impact tests. In: 19th International Offshore and Polar Engineering Conference, 21–26 June 2009, Osaka, Japan, pp. 125–134.

Kaplan, P., 1987. Analysis and prediction of flat bottom slamming impact of advanced marine vehicles in waves. International Shipbuilding Progress 34 (391), 44–53.

Kaplan, P., 1992. Wave impact forces on offshore structures: re-examination and new interpretations. In: Offshore Technology Conference, 4–7 May 1992, Houston, TX, USA.

Kapsenberg, G.K., 2011. Slamming of ships: where are we now?. Philosophical Transactions of the Royal Society A 369, 2892–2919.

Khabakhpasheva, T., Korobkin, A., 2013. Elastic wedge impact onto a liquid surface: Wagner's solution and approximate models. Journal of Fluids and Structures 36, 32–49.

Khabakhpasheva, T., Korobkin, A., Malenica, S., 2013. Fluid impact onto a corrugated panel with trapped gas cavity. Applied Ocean Research 39, 97–112.

Korobkin, A., 2003. Cavitation in liquid impact problems. In: 5th International Symposium on Cavitation, 1–4 November 2003, Osaka, Japan.

Korobkin, A., Malenica, S., 2005. Modified Logvinovich model for hydrodynamic loads on asymmetric contours entering water. In: 20th International Workshop on Water Waves and Floating Bodies, 29 May–1 June 2005, Longyearbyen, Norway.

Korobkin, A.A., 1996. Water impact problems in ship hydrodynamics. In: Ohkusu, M. (Ed.), Advances in Marine Hydrodynamics, Computational Mechanics Publications, pp. 323–371.

Korobkin, A.A., 2004. Analytical models of water impact. European Journal of Applied Mathematics 15, 821–838.

Korobkin, A.A., 2005. Three-dimensional nonlinear theory of water impact. In: 18th International Congress of Mechanical Engineering, 6–11 November 2005, Ouro Preto, MG.
Korobkin, A.A., 2006. Two-dimensional problem of the impact of a vertical wall on a layer of a partially aerated fluid. Journal of Applied Mechanics and Technical Physics 47 (5), 643–653.
Korobkin, A.A., 2011. Semi-analytical approach in generalized Wagner model. In: 26th International Workshop on Water Waves and Floating Bodies, 17–20 April 2011, Athens, Greece.
Lin, M., Shieh, L., 1997. Flow visualization and pressure characteristics of a cylinder for water impact. Applied Ocean Research 19, 101–112.
Oger, G., Doring, M., Alessandrini, B., Ferrant, P., 2006. Two-dimensional SPH simulations of wedge water entries. Journal of Computational Physics 213 (2), 803–822.
Oliver, J.M., 2002. Water Entry and Related Problems. D.Phil. Thesis, St Anne's College, University of Oxford, UK.
Peregrine, D.H., 2003. Water-wave impact on walls. Annual Review of Fluid Mechanics 35, 23–43.
Piro, D., Maki, K., 2011. Hydroelastic wedge entry and exit. In: 11th International Conference on Fast Sea Transportation, 26–29 September 2011, Honolulu, HI, USA.
Piro, D., Maki, K., 2012. Water exit of a wedge-shaped body. In: 27th Workshop on Water Waves and Floating Bodies, 22–25 April 2012, Copenhagen, Denmark.
Piro, D.J., Maki, K.J., 2013a. An Adaptive Interface Compression Method for Water Entry and Exit. Technical Report 2013-350, University of Michigan, Department of Naval Architecture and Marine Engineering. URL: ⟨http://deepblue.lib.umich.edu/handle/2027.42/97021⟩.
Piro, D.J., Maki, K.J., 2013b. Hydroelastic analysis of bodies that enter and exit water. Journal of Fluids and Structures 37, 134–150.
Qian, L., Causon, D.M., Mingham, C.G., Ingram, D.M., 2006. A free-surface capturing method for two fluid flows with moving bodies. Proceedings of the Royal Society A 462, 21–42.
Qin, H., Zhao, L., Shen, J., 2011. A modified Logvinovich model for hydrodynamic loads on an asymmetric wedge entering water with a roll motion. Journal of Marine Science and Application 10, 184–189.
Reinhard, M., 2013. Free Elastic Plate Impact into Water. Ph.D. Thesis, University of East Anglia, UK.
Reinhard, M., Korobkin, A., Cooker, M.J., 2011. Elastic plate impact onto water at high horizontal speed. In: 26th Workshop on Water Waves and Floating Bodies, 17–20 April 2011, Athens, Greece.
Reis, P.M., Jung, S., Aristoff, J.M., Stocker, R., 2010. How cats lap: water uptake by felis catus. Science 330, 1231–1234.
Scolan, Y.-M., 2004. Hydroelastic behaviour of a conical shell impacting on a quiescent-free surface of an incompressible liquid. Journal of Sound and Vibration 277, 163–203.
Scolan, Y.-M., Korobkin, A.A., 2001. Three-dimensional theory of water impact. Part 1. Inverse Wagner problem. Journal of Fluid Mechanics 440, 293–326.
Seddon, C.M., Moatamedi, M., 2006. Review of water entry with applications to aerospace structures. International Journal of Impact Engineering 32 (7), 1045–1067.
Semenov, Y.A., Yoon, B.-S., 2009. Onset of flow separation for the oblique water impact of a wedge. Physics of Fluids 21, 112103.
Takagi, K., 2004. Numerical evaluation of three-dimensional water impact by the displacement potential formulation. Journal of Engineering Mathematics 48, 339–352.
Tassin, A., Jacques, N., El Malki Alaoui, A., Nême, A., Leblé, B., 2010. Assessment and comparison of several analytical models of water impact. International Journal of Multiphysics 4, 125–140.
Tassin, A., Jacques, N., El Malki Alaoui, A., Nême, A., Leblé, B., 2012. Hydrodynamic loads during water impact of three-dimensional solids: modelling and experiments. Journal of Fluids and Structures 28, 211–231.
Techet, A., Truscott, T., 2011. Water entry of spinning hydrophobic and hydrophilic spheres. Journal of Fluids and Structures 27 (5–6), 716–726.
Toso, N.R.S., 2009. Contribution to the Modelling and Simulation of Aircraft Structures Impacting on Water. Ph.D. Thesis, Universität Stuttgart, Germany.
Truscott, T., Beal, D., Techet, A., 2009. Shallow angle water entry of ballistic projectiles. In: 7th International Symposium on Cavitation—CAV2009, 17–22 August 2009, Ann Arbor, MI, USA.
Tveitnes, T., Fairlie-Clarke, A., Varyani, K., 2008. An experimental investigation into the constant velocity water entry of wedge-shaped sections. Ocean Engineering 35, 1463–1478.
Ubbink, O., Issa, R., 1999. A method for capturing sharp fluid interfaces on arbitrary meshes. Journal of Computational Physics 153 (1), 26–50.
von Karman, T., 1929. The impact on seaplane floats during landing. NACA Technical Note 321.
Vorus, W., 1996. A flat cylinder theory for vessel impact and steady planing resistance. Journal of Ship Research 40, 89–106.
Vorus, W., 2004. A compliant-hull concept for planing craft wave-impact shock reduction. Journal of Engineering Mathematics 48, 253–277.
Wagner, H., 1931. Landing of seaplanes. NACA Technical Memorandum 622.
Wagner, H., 1932. Über Stoß- und Gleitvorgänge an der Oberfläche von Flüssigkeiten. ZAMM 12, 193–215. (in German).
Zhao, R., Faltinsen, O., Aarsnes, J., 1997. Water entry of arbitrary two-dimensional sections with and without flow separation. In: 21st Symposium on Naval Hydrodynamics. National Academy Press, Trondheim, Norway, pp. 408–423.